

AD-A132 118

EXPERIMENTAL RESEARCH ON RAIL VEHICLE SAFETY USING
DYNAMICALLY SCALED MODELS(U) PRINCETON UNIV N J DEPT OF
AEROSPACE AND MECHANICAL SCIENCES L M SWEET 1976

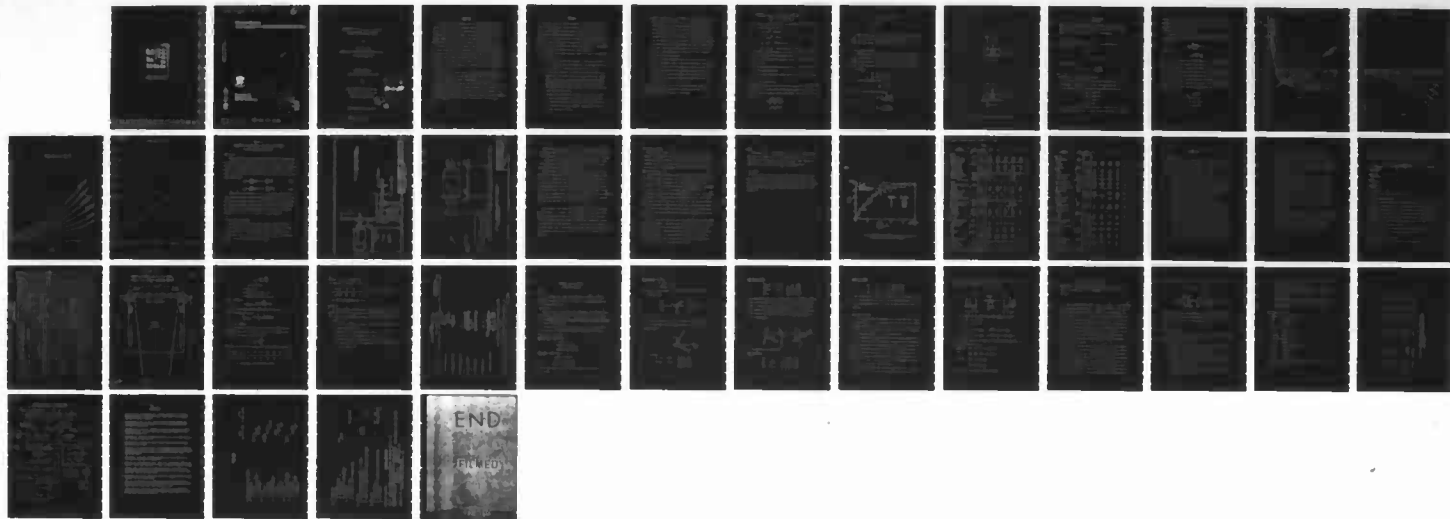
1/1

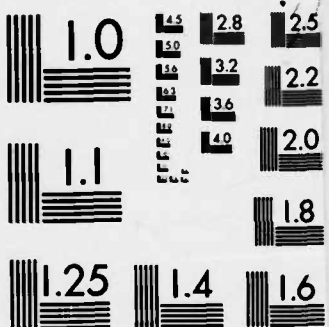
UNCLASSIFIED

PUAMS-1312 DOT-OS-60147

F/G 13/6

NL





MICROCOPY RESOLUTION TEST CHART
NATIONAL BUREAU OF STANDARDS-1963-A

AMS Report # 1312

①3

Princeton University

ADA132118

GR-1



PROPERTY
OF THE
ENGINEERING LIBRARY
REFERENCE COLLECTION

Department of
Aerospace and
Mechanical Sciences

DTIC FILE COPY

SD DTIC
SELECTED
SEP 07 1983
E

This document has been approved
for public release and sale; its
distribution is unlimited.

83 09 02 076

EXPERIMENTAL RESEARCH ON RAIL VEHICLE SAFETY
USING DYNAMICALLY SCALED MODELS

by

Larry M. Sweet

Department of Aerospace and Mechanical Sciences
Princeton University

Quarterly Report I

June 25, 1976-September 25, 1976

for

U.S. Department of Transportation

Office of University Research

Contract No. DOT-OS-60147

Accession For	
NTIS GRA&I	<input checked="" type="checkbox"/>
DTIC TAB	<input type="checkbox"/>
Unannounced	<input type="checkbox"/>
Justification	
<i>On file</i>	
By _____	
Distribution/	
Availability Codes	
Dist	Avail and/or Special
A	



AMS Technical Report NO. 1312

This document has been approved
for public release and sale; its
distribution is unlimited.

OBJECTIVE

The objectives of this research are to develop experimental techniques for the study of rail vehicle dynamics through the use of scaled models on tangent track, and to develop a structured experimental data base on the characteristics of rail car trucks. The complex interactions between track, wheels, suspensions, and vehicles are the causes of derailments, rapid deterioration of vehicle and track components, poor passenger and freight ride quality, and low operating speeds. These problems are significant because of the massive capital expenditures presently required for equipment rehabilitation to restore efficient and reliable operation. The establishment of a larger and more systematically structured experimental data base than that feasible from full-scale testing will enable the validation of analytical tools useful in design and evaluation of alternative technologies and safety criteria.

The experimental program consists of static and dynamic measurements of rail vehicle trucks at scaled speeds of up to 200 mph. Dynamic similitude in the one-fifth scale model (approximately twelve-inch gauge) is achieved by substituting a material with low elastic modulus for steel at the wheel/rail contact surfaces. Complex nonlinear dynamic phenomena, such as truck hunting, limit cycle oscillations, and incipient derailment, will be examined in controlled tests, and compared with results from theoretically derived simulation models and evidence from experiments on full-scale vehicles.

SUMMARY

The scope of work during the first year of the program (June 29, 1976-June 28, 1977) includes: (1) the design and fabrication of a scale model track, single wheelset, test carriage, and associated instrumentation; (2) measurement of wheelset displacement-force characteristics at steady velocity; (3) measurement of wheel-climb phenomenon; and (4) comparison of measured results with theoretical predictions. The results of this work will be applied to the design of a complete scale model truck and measurement of its static and dynamic stability characteristics.

→ The following activities have been completed during the first quarter of the program year:

- a) Design study of similitude parameters to determine model scale to be used over the course of the program. The selected track gauge is 12 inches, or a geometric scale factor of $A \approx 0.2$.
- b) Experimental measurement of lateral and tangential creep characteristics of LEXAN wheels and rails using a roller rig. LEXAN has been selected as a substitute for steel to achieve dynamic similitude in the critical creep forces. Comparisons of test data with theoretical models shows that LEXAN exactly reproduces creep forces in model scale.
- c) Design of the track support structure and rail system. Static and dynamic deflections were analyzed in detail; the stiffness, cost of fabrication, and availability of standard section shapes were included in a tradeoff analysis. Construction of the track structure has been initiated.

- c) Design of wheelset carriage, linkage, and instrumentation systems.

Various experimental configurations were investigated considering rail, wheelset, and contact plane coordinate systems, optional locations for force application, and allowed degrees-of-freedom. The investigation resulted in selection of applied and measured variables, and led to the development of the computational structure for our theoretical model. We are now conducting a simulated experiment "on-paper" to determine the full range of experimental variables. The results of the simulated experiment will be used to design instrumentation and to select experimental conditions for tests on the tangent track.

- e) Directory listing of potential users of the research results. A list of 29 potential users in the railroad technical community has been submitted to DOT for comment or addition. Formal contact has been established with 14 professionals in the field on a quarterly basis; useful correspondance in the form of technical reports or informal comments have been received from eight individuals to date.

A detailed description of Items a) through e) follows below. Also included are a work plan, assignment of personnel activities, and outline of activities for the second quarter of the program.

CALCULATION OF SCALE FACTORS FOR DYNAMICALLY SIMILAR
RAIL VEHICLE TRUCK MODELS

All scaling laws are defined by defining scale factors for length (λ), mass (λ_m), and time (λ_T); therefore:

$$\lambda_V = \lambda \lambda_T^{-1} \text{ (velocity)} \quad (1a)$$

$$\lambda_F = \lambda \lambda_m \lambda_T^{-2} \text{ (force)} \quad (1b)$$

$$\lambda_K = \lambda_m \lambda_T^{-2} \text{ (spring constant)} \quad (1c)$$

$$\lambda_E = \lambda^{-1} \lambda_m \lambda_T^{-2} \text{ (elastic modulus or stress)} \quad (1d)$$

The selection of scale factors λ , λ_m , and λ_T for the Princeton experiments is governed by the following considerations:

- a) Goal of simulating truck dynamics up to scaled speeds of 330 km/hr (200 mph).
- b) Limitation of Princeton Dynamic Model Track to operating speeds of 12.2 m/sec(40 feet/sec).
- c) Properties of materials suitable for fabrication of truck components.

Scaling the Creep Coefficient:

The creep coefficient f can be shown to be proportional to $G^{1/3} N^{2/3} r^{2/3}$, where G , N , and r are the material shear modulus, applied normal force, and wheel/rail geometry parameter, respectively [1,4]. If the model is dynamically scaled, then

$$\begin{aligned} \frac{f}{f_0} &= \frac{G^{1/3} N^{2/3} r^{2/3}}{G_0^{1/3} N_0^{2/3} r_0^{2/3}} \\ &= \lambda_G^{1/3} \lambda_N^{2/3} \lambda_r^{2/3} \end{aligned} \quad (2)$$

$$\begin{aligned}
 &= (\lambda^{-1} \lambda_m \lambda_T^{-2})^{1/3} (\lambda \lambda_m \lambda_T^{-2})^{2/3} \lambda^{2/3} \\
 &= \lambda \lambda_m \lambda_T^{-2} \\
 &= \lambda_F
 \end{aligned}$$

Equation (2) requires a scaling of shear modulus by λ_G , as was recognized in [7]. For two materials of equal Poisson's ratio ν , the scale factors for shear modulus and Young's modulus are equal.

Scaling the Wheel Loading:

Consider full-scale and model trucks shown in Figure 1. The applied load \bar{N}_0 in full-scale is one-half the vehicle body weight plus body dynamic loading; the applied load \bar{N} in the model experiment is a free variable to be set equal to the scaled value of \bar{N}_0 . The total load carried by the wheels is then,

$$N_0 \equiv m_0 g + \bar{N}_0 \quad (\text{full-scale}) \quad (3)$$

$$N \equiv m g + \bar{N} \quad (\text{model}) \quad (4)$$

Defining dimensionless force ratios,

$$n \equiv \frac{\bar{N}}{mg} \quad n_0 \equiv \frac{\bar{N}_0}{m_0 g} \quad (5)$$

we can enforce wheel load similitude as,

$$\lambda_F = \frac{N}{N_0} = \frac{\bar{N} + mg}{\bar{N}_0 + m_0 g} \quad (6)$$

which leads to

$$\lambda_T^2 = [\lambda \frac{(1 + n_0)}{(1 + n)}]$$

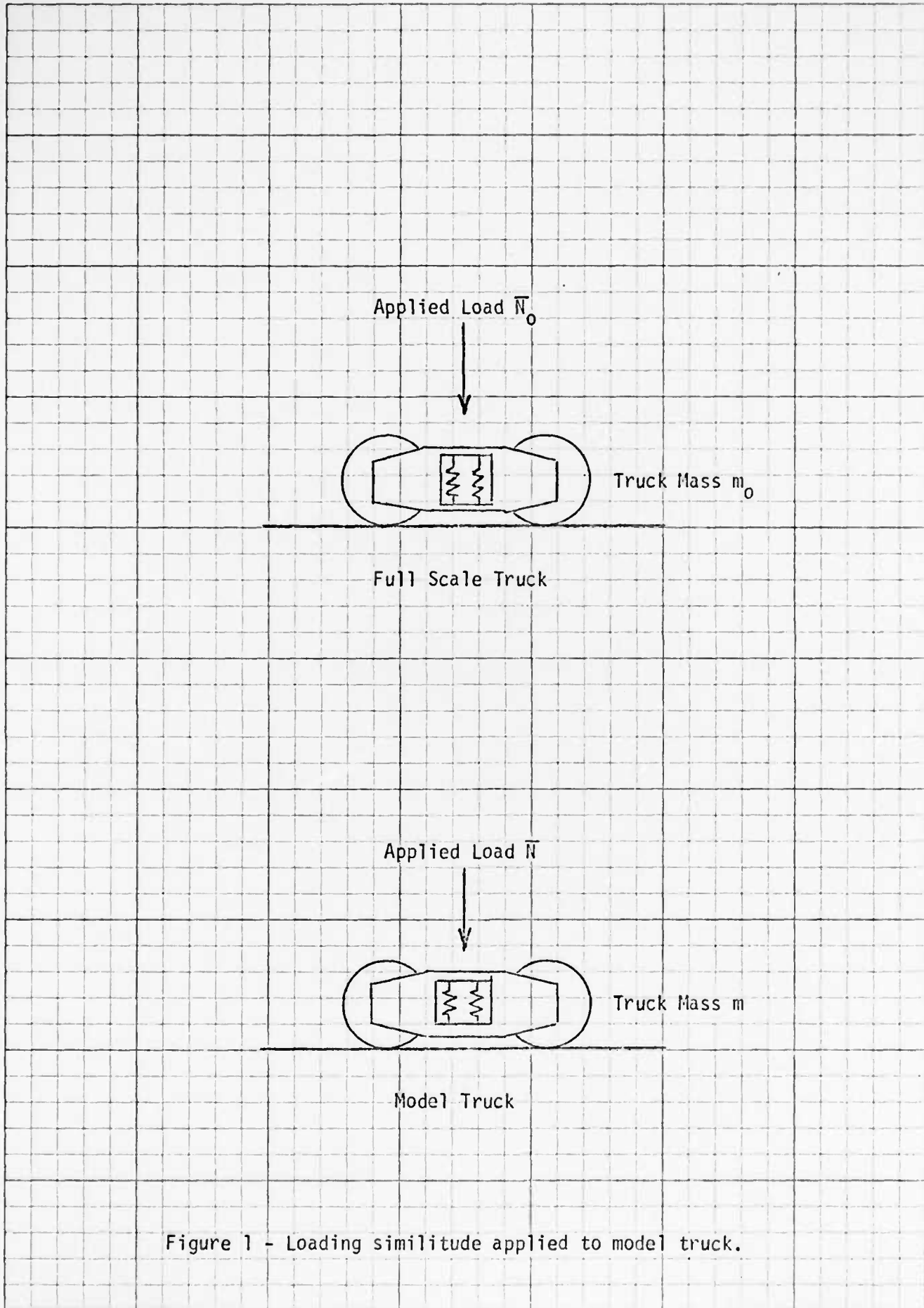


Figure 1 - Loading similitude applied to model truck.

or

$$\lambda_V = \left[\lambda \frac{(1+n)}{(1+n_0)} \right]^{1/2} \quad (7)$$

Equation (7) establishes the velocity scale law as a function of model geometric scale λ and applied load ratio n , since the full-scale applied load ratio n_0 is specified by the vehicle being modeled.

Scaling the Truck Mass:

The truck mass M is determined by the model material density ρ and the force scaling law,

$$\lambda_m \equiv \lambda_p \lambda^3 \quad (8)$$

$$\lambda_F \equiv \lambda_G \lambda^2 = \lambda_m \lambda \lambda_T^{-2} \quad (9)$$

Using (6) establishes,

$$\lambda_m = \lambda_G \lambda^2 \frac{(1+n_0)}{(1+n)} \quad (10)$$

Determination of Model Design Parameters:

The scaling is determined by the selection of model size, wheel and rail material, and applied force ratio. For a double bolster truck of British Railways [9], the following load parameters were determined,

$$m_0 g = 13,163 \text{ lbs.}$$

$$\bar{N}_0 = 31,380 \text{ lbs.}$$

$$N_0 = 44,543 \text{ lbs.}$$

$$n_0 = 2.384$$

Applying Equation (7) yields the plots in Figure 2 of model load ratio n for various maximum full-scale velocities and model sizes. Models

in range $0.1 < \lambda < 0.25$ are of greatest practical interest, indicating the necessity of "off-loading" the model; this is readily accomplished by applying a pre-tension in the secondary suspension springs placed between the truck and idler carriage.

A polycarbonate resin LEXAN 141, manufactured by General Electric Co., has been selected for fabrication of the wheel treads and rails. For the above model,

$$\lambda_G = \frac{G_{\text{LEXAN}}}{G_{\text{STEEL}}} = 0.012$$

From (8) and (10),

$$\lambda_p = \frac{0.0406}{\lambda} \left(\frac{1}{1+n} \right) \quad (11)$$

The truck model density can be made different from that of LEXAN by fabricating the truck frame, wheelset axles, wheel hubs, etc., out of any material. For $\lambda = 0.2$, aluminum is a convenient choice.

Applying the selected scale factors to the truck in [9] yields plots in Figures 3-5 of truck weight mg , applied load \bar{N} , and total load N for various values of λ and $V_{o_{\max}}$. We have selected a track gauge of 12 inches, or a scale factor of $\lambda \approx 0.2$, for our experiments. The particular scaled speed and applied model loads used will be dependent on the truck configuration tested; for example,

$$V_{o_{\max}} = 200 \text{ mph}$$
$$mg = 68.0 \text{ lbs.}$$

$$\bar{N} = -46.5 \text{ lbs.}$$

$$il = 21.5 \text{ lbs.}$$

PLOT OF n VS. λ

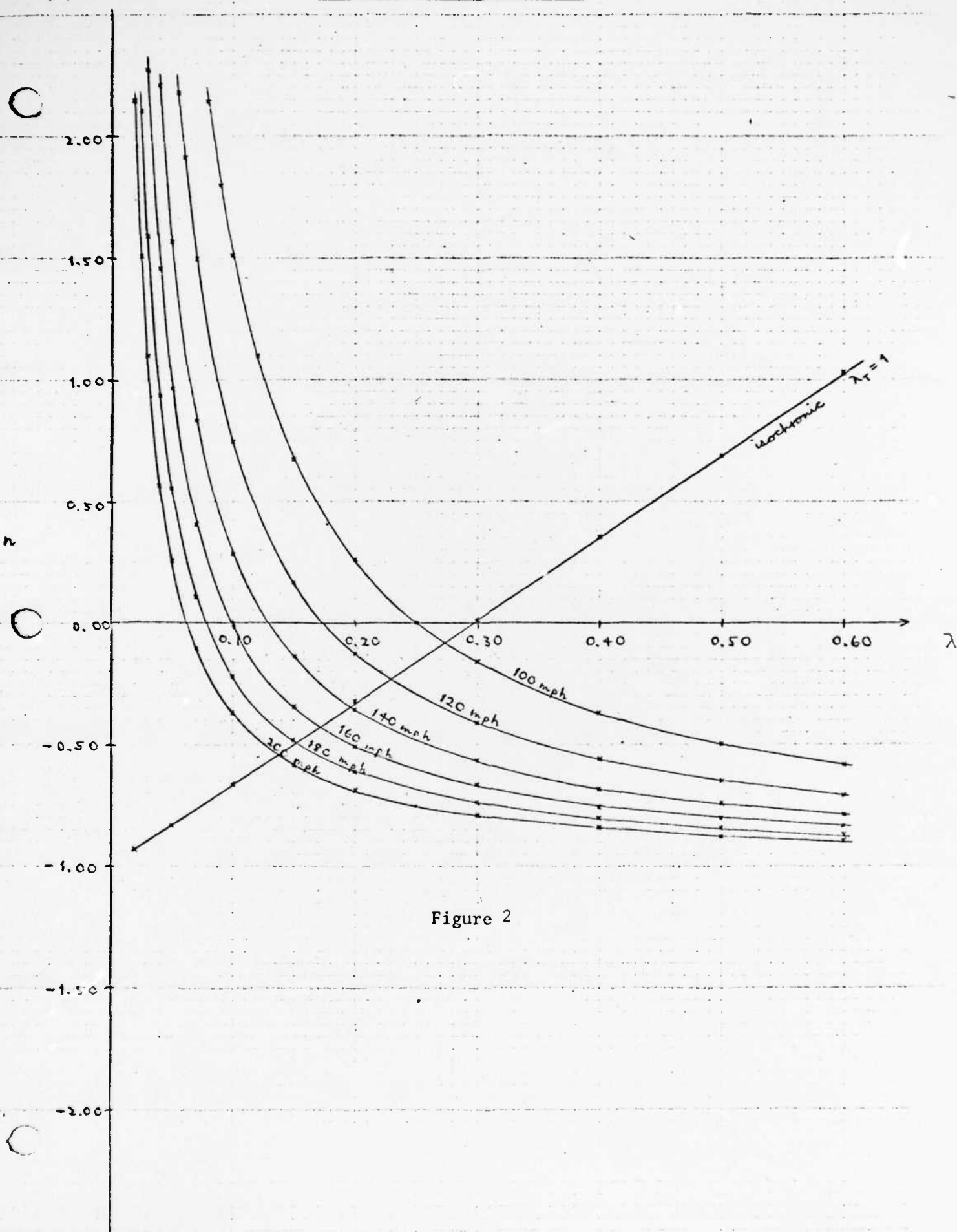


Figure 2

~~WERTEN TEL~~

PLOT OF \bar{K} VS. λ

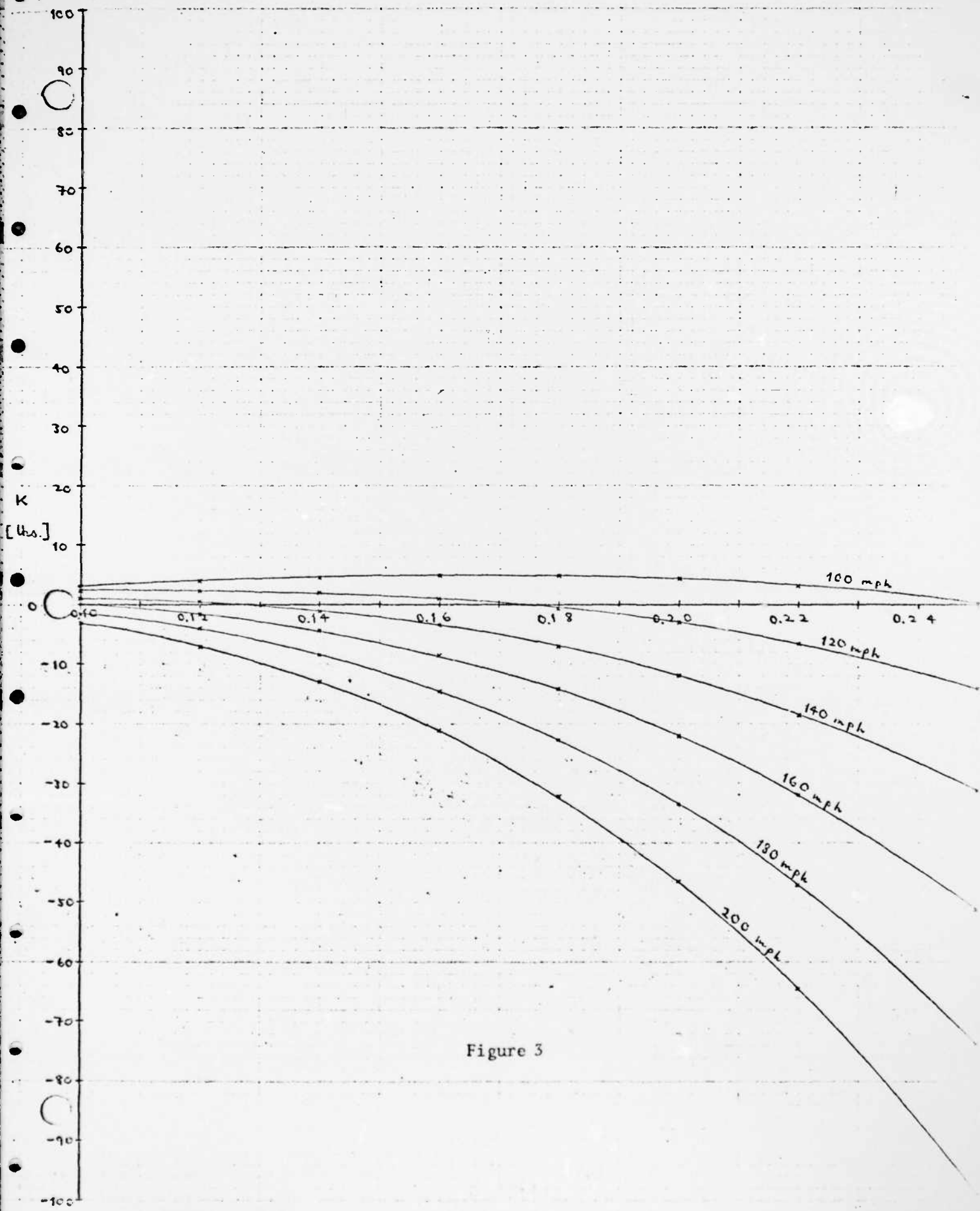


Figure 3

M_g [Abs.]

PLOT OF M_g VS. λ

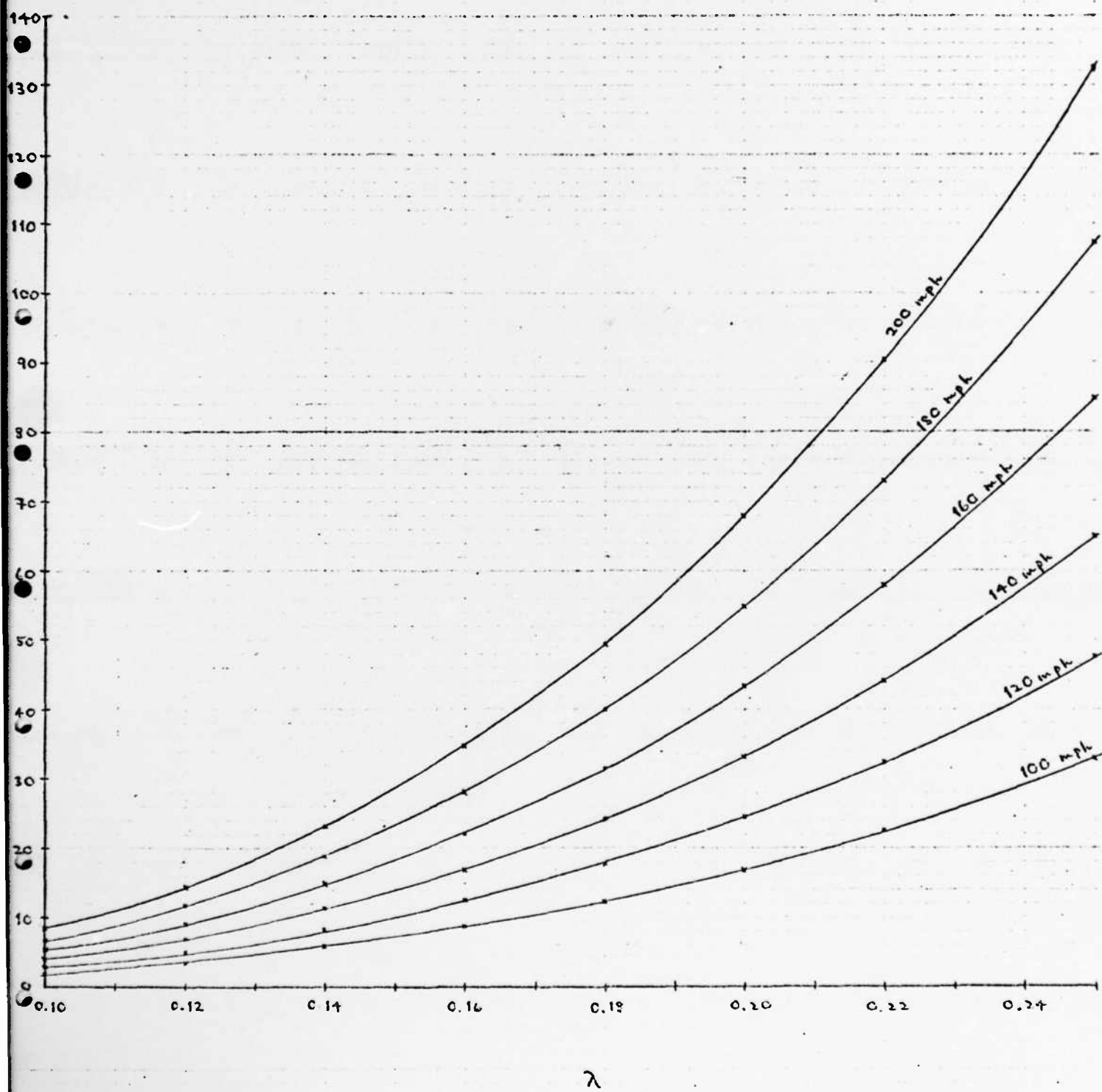


Figure 4

~~4500 N~~

PLOT OF N vs. λ

N [U.S.]

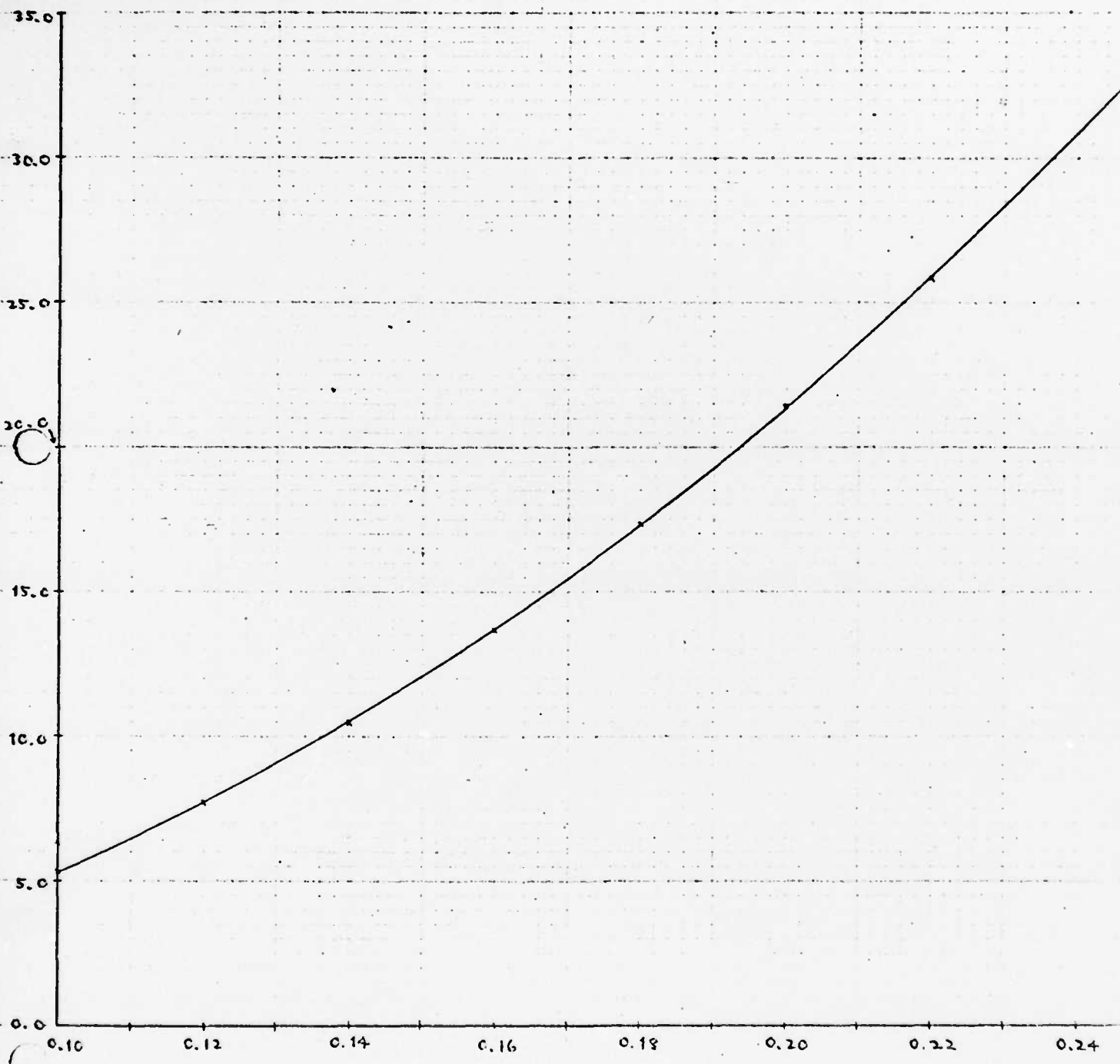


Figure 5

ROLLER RIG
MEASUREMENT OF LONGITUDINAL AND LATERAL CREEP FORCES
BETWEEN LEXAN WHEELS AND RAILS

Objective:

Theoretical studies relating the forces generated in the contact plane to the applied normal force and relative slip have shown a functional dependence of the creep phenomenon on the properties of the materials in contact. Specifically, the material shear modulus G or elastic modulus E , Poisson's ratio ν , and coefficient of sliding friction μ are necessary to define the creep formula [1].

$$\xi_x = -\frac{3\mu N}{G_{\text{stab}}} \phi \left[1 - \left(1 - \frac{F_x}{\mu N} \right)^{1/3} \right] \quad (12)$$

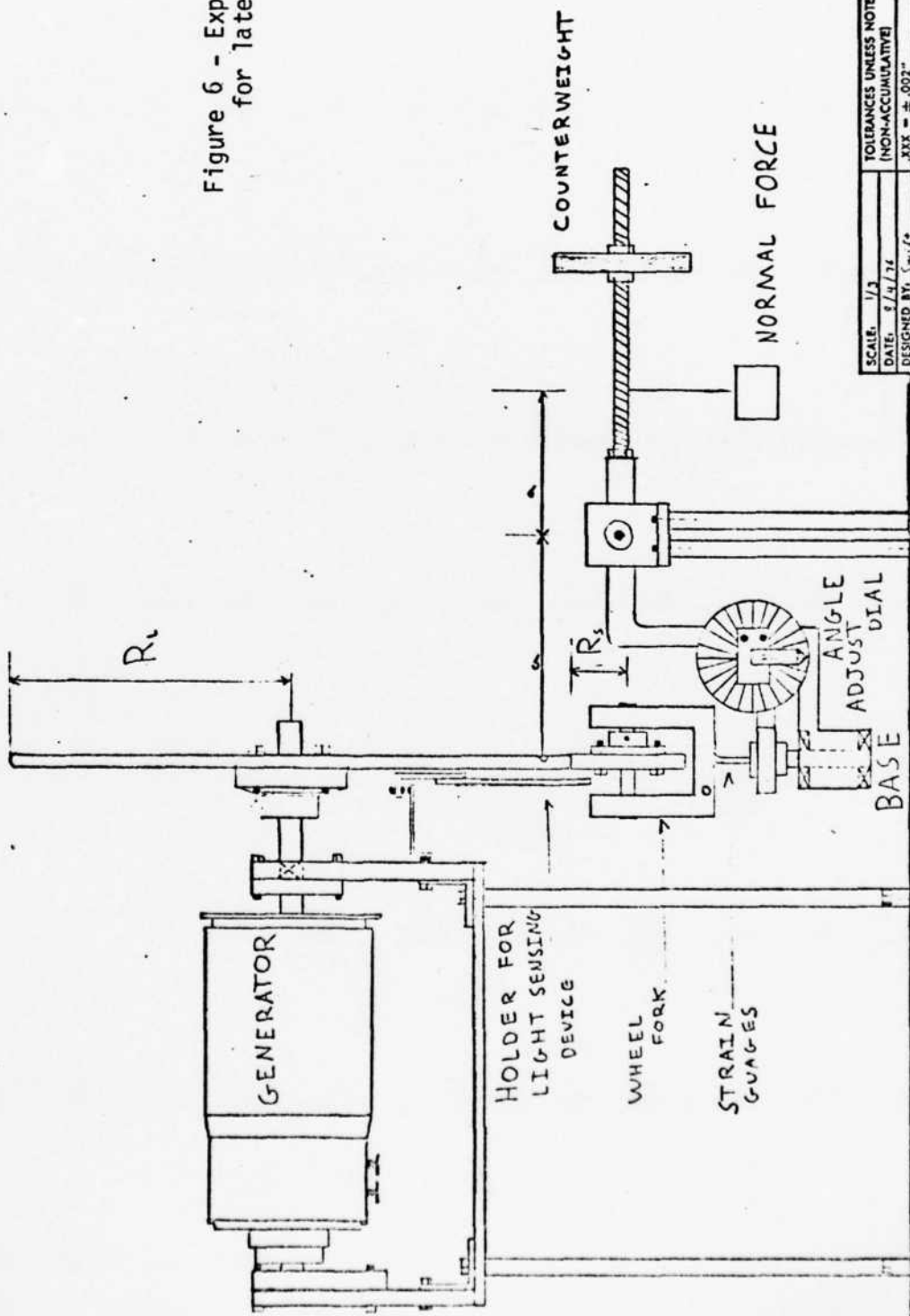
$$\xi_y = -\frac{3\mu N}{G_{\text{stab}}} \psi_1 \left[1 - \left(1 - \frac{F_y}{\mu N} \right)^{1/3} \right] \quad (13)$$

The objective of the roller rig tests was to establish the validity of using LEXAN to reproduce dynamically scaled wheel/rail creep forces. LEXAN was selected because of its modulus ratio with respect to steel, excellent machinability, toughness, and dimensional stability, and high coefficient of sliding friction (in comparison with many other polymer materials). A summary of relevant mechanical properties is given in Table 1.

Description of Experiments:

The apparatus used to measure lateral creep is shown in Figure 6. The rail, whose radius is approximately five times larger than the radius of the small wheel, is driven by a General Motors Delco-Remy generator functioning as a motor. The two wheels are kept in contact with each other by means of a counter-weight on the small wheel.

Figure 6 - Experimental apparatus
for lateral creep measurements.



SCALE:	1/2	CHANGE	BY	APP.
DATE:	9/4/74	TOLERANCES UNLESS NOTED (NON-ACCUMULATIVE)	NO. PROD.	
DESIGNED BY:	S. S.	XXX = $\pm .002"$	MATERIAL	
DRAWN BY:	F. L.	XX = $\pm .005"$	FINISH UNLESS NOTED:	✓
CHECKED BY:		FRACTIONS = $\pm 1/64"$	TITLE:	
APPROVED BY:		ANGLES = $\pm 1^{\circ}$		

FLIGHT MECHANICS LABORATORY
DEPARTMENT OF MATHEMATICAL ENGINEERING
JOHNS HOPKINS UNIVERSITY
BALTIMORE, MD 21214

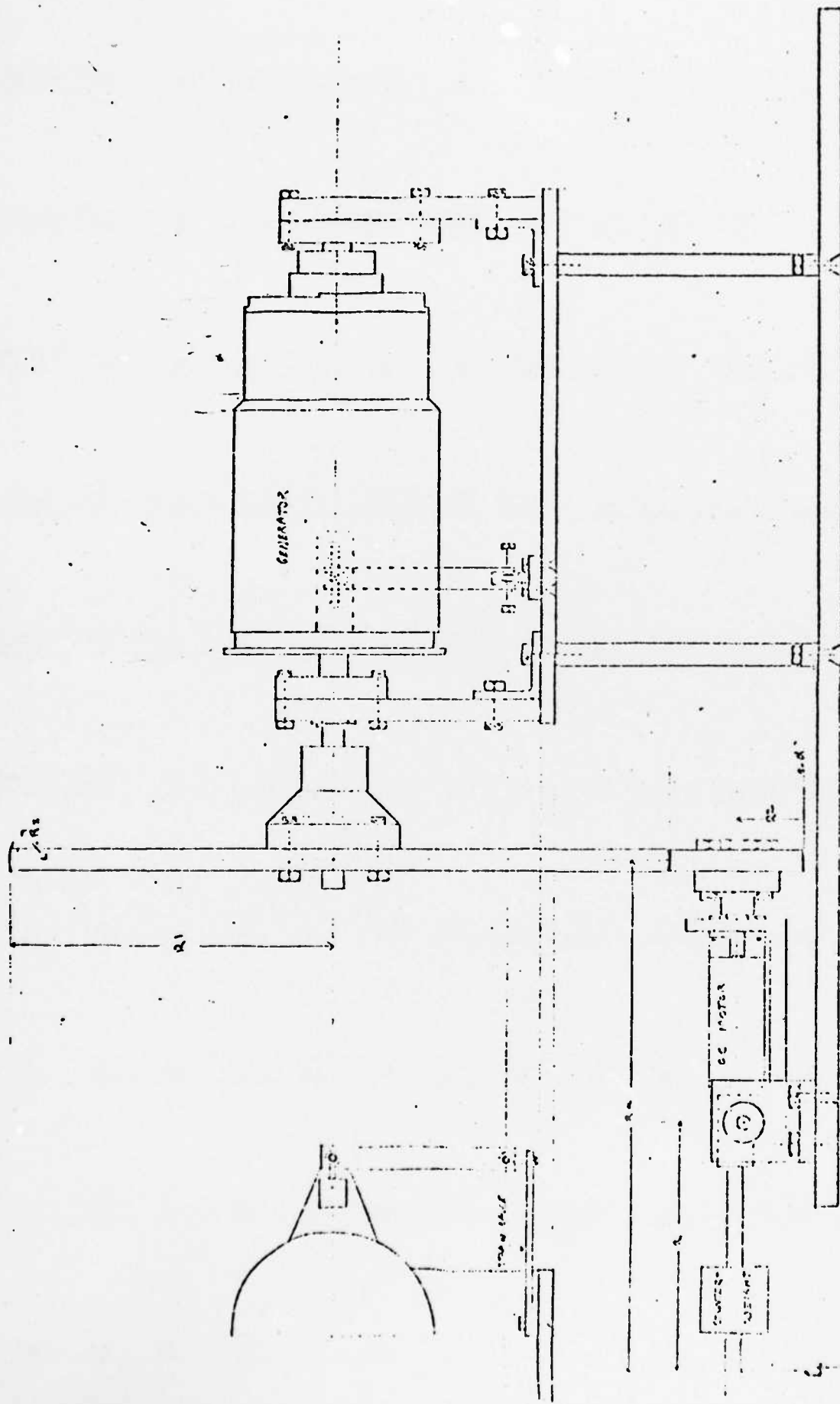


Figure 7 - Experimental apparatus for tangential creep measurements.

SC. 6	RECEIVED MAY 10 1943	NO. 1
DATE	SEARCHED INDEXED	SEARCHED
DRAWN BY	FILED	INDEXED
DRAWN IN	MAILED	FILED
CHIEF EXP.	PRINTED	PRINTED
EX-100	1943	1943

FIREWALL MECHANICS LABORATORY
BUREAU OF FIRE ENGINEERING
PRINCETON UNIVERSITY

Wheel and rail translational velocities are determined by measurement of rotational periods of wheel and rail. The device used involved actuation of two Monsanto MCA7 reflective object sensors by single strips of aluminum mounted near the outer edge of each wheel. The intensified signals drive independent circuits and counters. The velocity of the rail was controlled by varying the voltage to the generator.

The small wheel is mounted on a wheel fork that allows the relative angle between the two wheel surfaces to be manipulated accurately by means of two screws mounted on either side of a handle attached to the base of the fork. By turning the screws which push the handle, the fork can turn on its bearings, which are mounted in the base of the movable arm (which has bearings of its own). Readings are taken with a dial calibrated in intervals of 0.03° of angle between the two wheels. The lateral force was measured by strain gages mounted on the "neck" of the wheel fork. Lateral creep is calculated from the wheel velocities and relative angle.

The tangential creep experiment was conducted on a similar apparatus, shown in Figure 7. To produce a relative tangential velocity both wheels were driven by electric motors with the wheel axles parallel. The motor driving the larger wheel was mounted in bearings and restrained by a strain gage load cell. The load measurement was then proportional to the desired tangential creep force. The velocity measurement, normal force application, and experimental procedure were similar to those used in the lateral creep measurements.

Experimental Results:

Plots of lateral creep forces versus relative velocity are shown in Figure 8. For each normal force the curves are plotted using the value for coefficient of sliding friction μ as measured at the associated full slip condition. We observed a slight decrease in μ with increasing normal force from 0.52 to 0.46. The magnitude of this trend is consistent with results reported in [2, 3, 5, 8].

The plotted data for lateral creep are quite repeatable if the wheels are cleaned with methanol prior to test. We observed a decrease in μ to less than 0.1 and a tenfold increase in slip when the wheels were allowed to accumulate oil, dust, and other contaminants. The magnitude of the contamination effects are also similar to those reported in [2, 5, 8].

The good correlation of experimental data with the theory of Vermeulen and Johnson [1] is equivalent to that typically obtained in careful steel wheel/steel rail experiments [1, 2, 3, 5]. The rms difference between theory and experimental data is 6.6% of full scale, with measurement error band of $\pm 4.4\%$. During the next quarter we plan to replace the Vermeulen and Johnson theoretical model with Kalker's creep coefficients, recomputed for a Poisson's ratio of $\nu = 0.5$.

We have encountered problems in obtaining repeatable data in the tangential creep experiments. The motors have non-linear characteristics, and the resistors used in the manually-controlled motor control circuits change resistance over time. Consequently it has proven difficult to control both motors simultaneously to maintain constant rail speed under the desired force and creep conditions. We may need to use velocity feedback control on the motors to perform the experiment satisfactorily.

Wear:

No significant wear was observed after several hours of operation with the roller rig. We anticipate tangent track wear to be minimal due to the distribution of load exposure over the track length. Wheel wear will be monitored using contact impression tape, as developed in [3].

Conclusion:

The results to date indicate that LEXAN is a suitable material for wheel/rail experiments, in that scaled creep forces are accurately reproduced. As is the case with any wheel/rail experiment the surface contamination is important, and thus will require regular cleaning prior to each experiment.

COMP

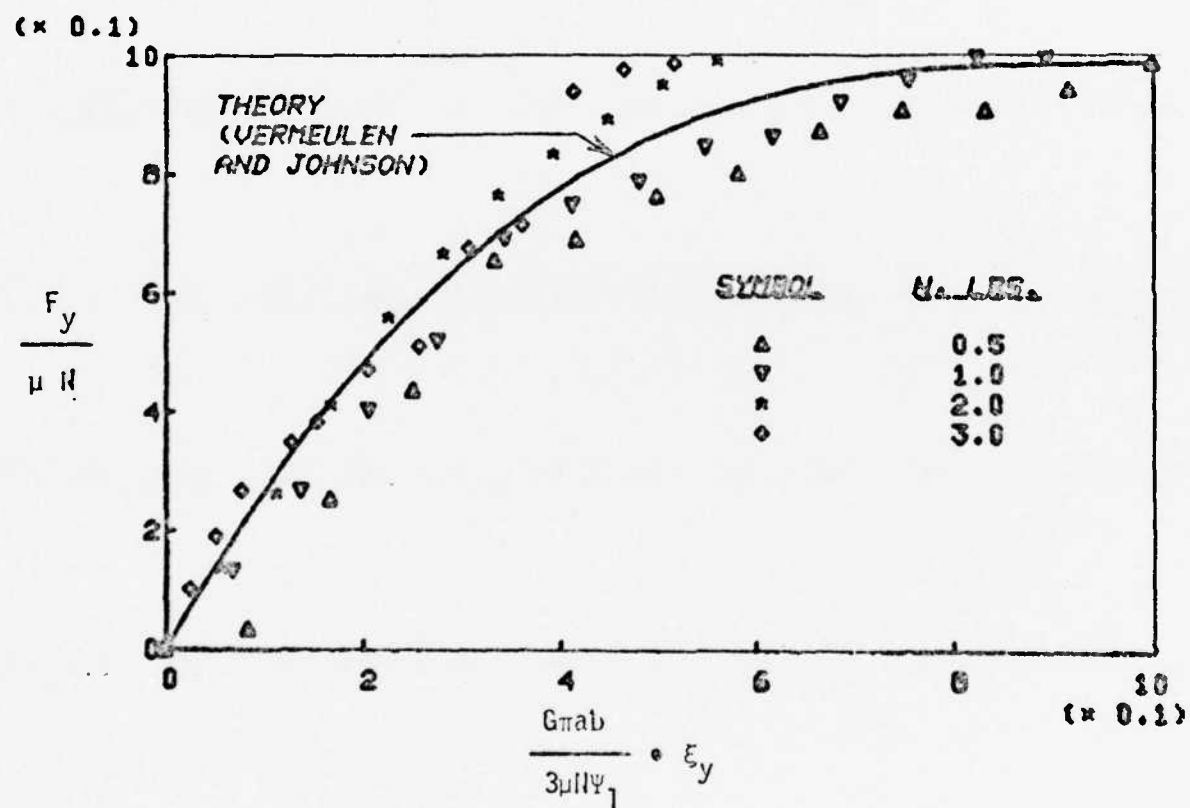


Figure 8 - Comparison of lateral creep force measurements with theory of Vermeulen and Johnson.

Typical Properties of LEXAN Resins

Table 1

PROPERTY	ASTM TEST METHOD	LEXAN 101, 141, 121	LEXAN 204	LEXAN 121	LEXAN 500	LEXAN 45	LEXAN 3412	LEXAN 3414
PHYSICAL								
Specific Gravity	D792	1.20	1.24	1.19	1.25	1.20	1.35	1.52
Specific Volume, in. ³ /lb.	-	23.1	22.3	23.3	22.2	23.1	20.5	18.2
Weight/volume, lbs./in. ³	-	0.043	0.045	0.043	0.045	0.043	0.040	0.035
Water Absorption, %	D570							
24 hrs. @ 73°F		0.15	0.15	0.19	0.12	0.15	0.16	0.12
Equilibrium, 73°F		0.35	0.32	0.37	0.31	0.35	0.29	0.23
Equilibrium, 212°F		0.58	0.53	0.54	-	0.53	-	-
Mold Shrinkage, in./in.	D955	0.005-0.007	0.005-0.007	0.005-0.007	0.002-0.004	0.005-0.007	0.002-0.003	0.001-0.002
Transmittance, % (Natural)	D1003	88-89	87-88	-	-	89	-	-
Haze, % (Natural)	D1003	1-2	1-2	-	-	1-2	-	-
THERMAL								
Heat Deflection Temperature, °F	D648							
At 66 psi		280	290	280	295	280	300	310
At 264 psi		270	270	260	233	270	295	235
Specific Heat, btu/lb./°F	-	0.30	-	-	-	0.30	-	-
Thermal Conductivity, btu/hr./ft. ² /°F/in.	-	1.35	1.35	-	1.41	1.35	1.47	1.53
Coefficient of Thermal Expansion, in./in./°F	D696	3.75×10^{-5}	3.75×10^{-5}	3.6×10^{-5}	1.79×10^{-5}	3.75×10^{-5}	1.49×10^{-5}	0.53×10^{-5}
Vicat Softening Temperature, °F	D1525	310-320	-	-	-	310-320	-	-
Brittleness Temperature, °F	D746	<-200	-	-	-	<-200	-	-
Flammability								
ASTM D635	D635	SE‡	SE	SB†	SE	SE	SE	SE
UL Subject 94	UL94	SE II	SE I	Burns	SE O	SE II	SE I	SE I
Oxygen Index	D2863	25.0	29.5	23.2	32.5	25.0	30.5	30.0
ELECTRICAL								
Dielectric Strength, volts/mil	D149							
Short time, 125 mils		380	380	415	450	380	490	450
Dielectric Constant	D150							
60Hz		3.17	3.17	-	3.10	3.17	3.17	3.53
10 ⁴ Hz		2.96	2.96	3.0	3.05	2.95	3.13	3.43
Power Factor	D150							
60Hz		0.0003	0.0003	0.0009	0.0003	0.0003	0.0003	0.0013
10 ⁴ Hz		0.010	0.010	0.0001	0.0075	0.010	0.0073	0.0037
Volume Resistivity, ohm-cm.	D150							
@ 73°F, dry		8.2×10^{14}	8.2×10^{14}	2.5×10^{14}	5.8×10^{14}	8×10^{14}	4.6×10^{14}	4.8×10^{14}
Arc Resistance, sec.	D495							
Stainless Steel Electrodes		10-11	10-11	10-11	5-10	10-11	5	5
Tungsten Electrodes		120	120	120	120	120	100	110

†Slow Burning ‡Self-extinguishing *Parts to 6" in length. 0.0025-0.0045 in./in. for parts 6" to 16" in length; 0.0055-0.0085 in./in. for parts greater than 16" in length

PROPERTY	ASTM TEST METHOD	TEXAN 101, 141, 121	TEXAN 2014	TEXAN 191	TEXAN 500	TEXAN 15	TEXAN 3112	TEXAN 3114
MECHANICAL								
Tensile Strength, psi	D638							
Yield		9,000	9,000	8,500	9,000	9,000	—	—
Ultimate		9,500	9,500	9,200	8,000	9,500	16,000	23,000
Elongation, %	D638							
Yield		6-8	6-8	6-8	8-9	6-8	—	—
Rupture		110	110	115	10-20	110	4-6	3-5
Tensile Modulus, psi $\times 10^3$	D638	3.45	3.45	3.39	4.50	3.45	8.60	15.60
Flexural Strength, psi	D790	13,500	13,500	11,800	15,000	13,500	19,000	27,000
Flexural Modulus, psi $\times 10^3$	D790	3.40	3.45	3.10	5.0	3.40	8.0	14.0
Compressive Strength, psi	D695	12,500	12,500	10,000	14,000	12,500	16,000	21,000
Compressive Modulus, psi $\times 10^3$	D695	3.45	3.45	3.34	5.20	3.45	7.60	15.00
Shear Strength, psi	D732							
Yield		6,000	6,000	—	8,500	6,000	10,000	11,000
Ultimate		10,000	10,500	8,500	—	10,000	—	—
Shear Modulus, psi $\times 10^3$	—	1.14	—	—	1.47	1.14	2.03	3.19
Izod Impact Strength, ft. lbs./in.	D256							
Notched, $\frac{1}{8}$ " thick		12-16	12	14	4-6	12-16	2.0	2.5
Unnotched, $\frac{1}{8}$ " thick		NF*	NF	NF	20-40	NF*	19	24
Tensile Impact Strength, ft. lbs./in. ²	D1822							
S-type		300	225	200	40	300	30	35
L-type		650	500	650	—	650	30	35
Falling Dart Impact Strength, ft. lbs., $\frac{1}{8}$ " thick	—	>125	>125	>125	>125	>125	2.5-5	3-6
Fatigue Strength, psi @ 2.5 mm cycles	D671	1,000	1,000	1,000	3,500	1,000	5,000	7,000
Rockwell Hardness	D785							
M		70	74	68	85	70	91	93
R		118	120	118	124	118	122	119
Deformation Under Load, %	D621							
4000 psi, @ 73°F		0.2	0.25	0.22	0.1	0.2	0.04	0.02
4000 psi, @ 153°F		0.3	0.5	—	—	0.3	0.10	0.05
Taber Abrasion Resistance, mg. weight loss/1000 cycles	D1044	10	9	20	11	10	17	32

*NF No Failures

GUIDEWAY DESIGN

Design Approach:

A significant effort has been devoted to the design of the guideway structure and rails, since this investment will literally be the foundation of several years of research. We desire a straight, smooth, and inflexible rail to isolate the truck dynamics for study. To this end the following design guidelines were used:

- a) Due to floor settlement, temperature gradients, relaxation of internal stresses in large section members, and other uncertainties, the guideway will consist of adjustable members, rather than trying to achieve tolerance goals on a single, fixed member. However, the presence of adjustment points may increase the probability of misalignment occurring over time.
- b) The static deformations under point loads (truck) and distributed loads (guideway weight) should be within the overall design tolerance. We have had to confront a direct tradeoff in section stiffness with manufacturing tolerance. In all cases the expected rolling or extruding mill tolerances had been determined and accounted for in the design. The calculated deflections that follow are conservative, assuming no transfer of shear stress across friction or bolted joints. Beams distributed in the longitudinal direction (semi-continuous, 3 span) were assumed to have 3/4 the deflections of simply supported beams. Beams distributed in three dimensions (rail retaining

angles, for example) were assumed to have a stiffness equivalent to a beam section with length equal to twice the beam height.

- c) Dynamic interaction between model and track is not permitted. To the end transit time ratios (pier crossing time to period of guideway fundamental frequency) of greater than 2.0 are required.
- d) Standard sections are to be used whenever possible, to minimize cost and delivery time.
- e) Thermal expansion is considered. The only significant design problem we have encountered with Lexan is that, in scale, it expands 30 times more than steel (x 6 in expansion coefficient). We are investigating several options to prevent large gaps at rail joints, such as maintaining the rails at constant temperature along the test section, and using expansion joints along acceleration and deceleration sections. Thermal buckling has been considered for the worst case of maximum ΔT and temperature control failure.
- f) The selection of bolt locations and spacing is critical to the cost of construction and alignment. We are currently developing a model following [10], to convert alignment tolerances into rail spectra. We are also looking at ways of quickly surveying the overall track profile, such as a California profilometer, to eliminate the need to perform periodic transit surveys.

The structure design is shown in Figure 9. Symbols used are AISC (American Institute of Steel Construction) and CRS (cold-rolled steel).

The status of the guideway construction phase is summarized below:

Element	Price		Price		
	Designed	Requested	Quoted	Ordered	Delivered
Steel Channel & Plate	X	X	X	X	X
Aluminum Extrusion	X	X	X		
Lexan Extrusion	X	X			
Guideway Studs	X	X	X		
Laser Transit	N.A.	X			

Static Deflection Analysis:

The static deflections were estimated assuming a worst case of 100 lbs. vertical load (maximum carriage + truck weight) and 100 lbs. lateral load applied dynamically on one rail. The structure is redundant; however in design we assumed zero load carried in shear by bolted joints. Under normal conditions (vertical load = 100 lbs., lateral load = 25 lbs.) we anticipate deflections of the order of 0.0025", which is within our design goal. The calculations are summarized in Table 2.

Deflections of the actual structure will be measured after the first sections are completed to determine the need for added stiffness.

Dynamic Deflections of Structure:

The dynamic interaction between vehicle and guideway is determined from the transit time ratio [11],

KOE 10X10 TO 1 INCH 3 X 1 INCHES
KELFEL & FISCH CO. MADE IN U.S.A.

461322

System

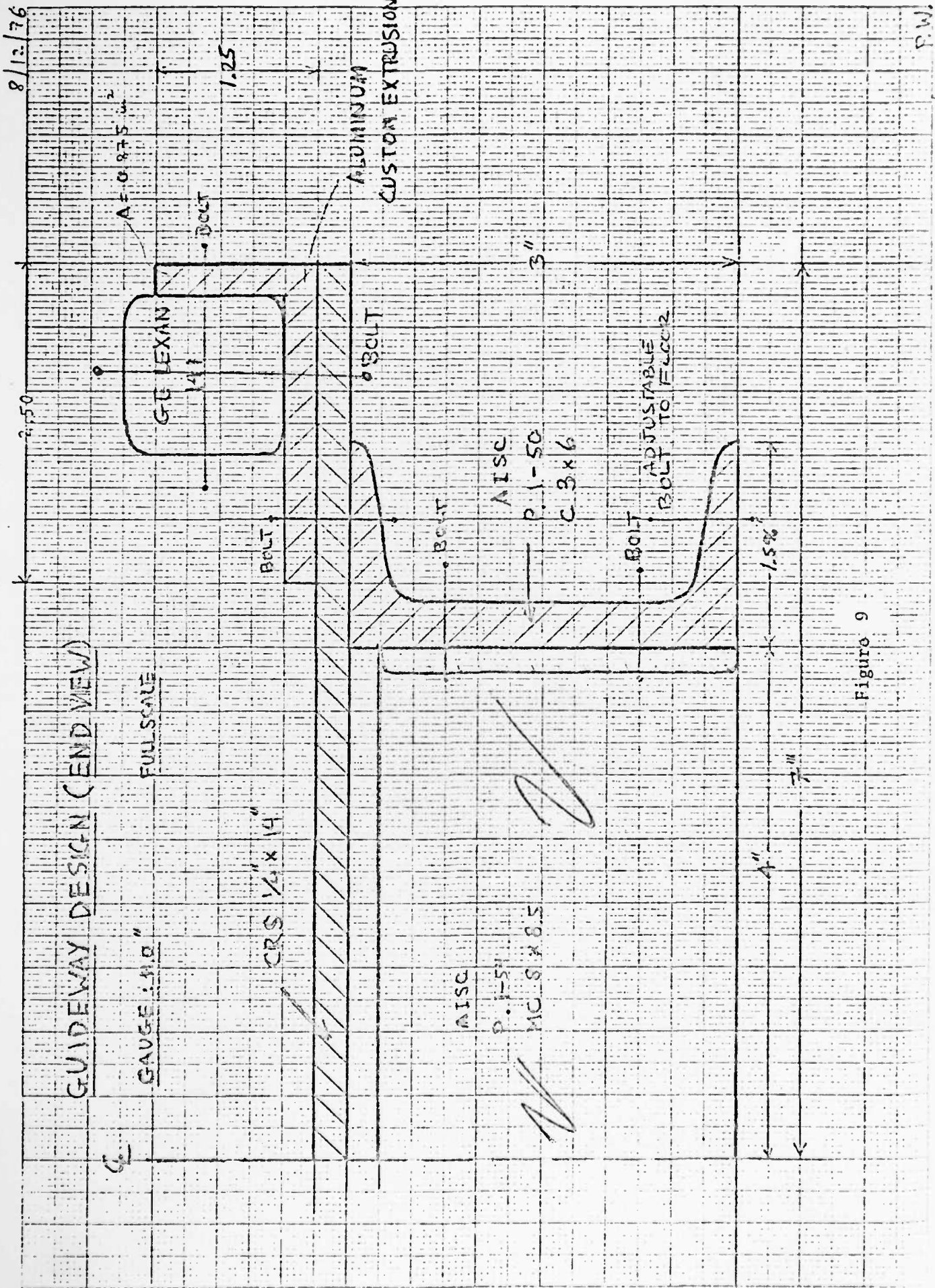
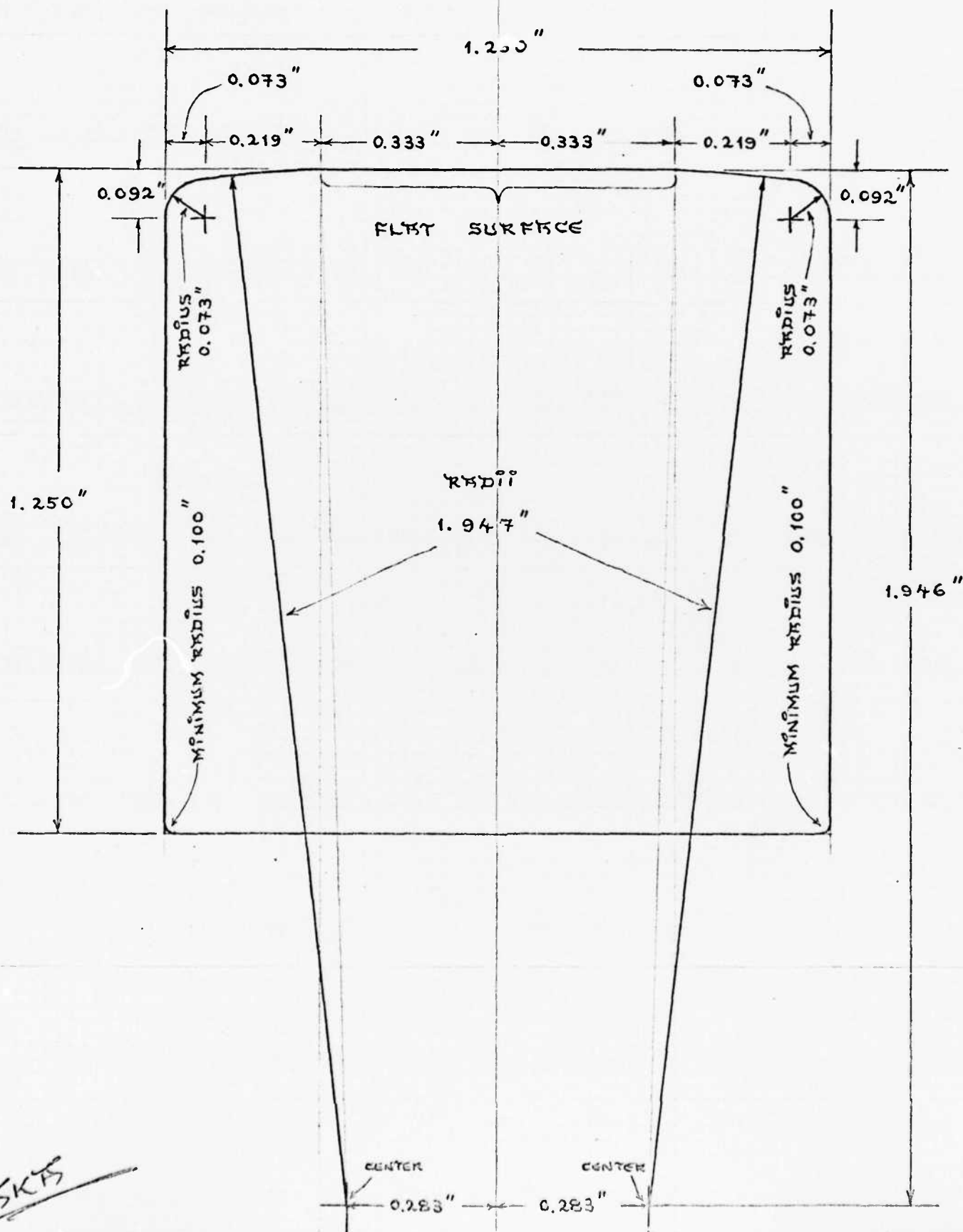


Figure 9

FIGURE 10

CROSS-SECTION OF LEXAN RISIL
(DRAWN 4 TIMES ACTUAL SIZE)

9/1/76.



$$T_{\text{transit}} = \frac{\pi}{2Vl} \sqrt{\frac{EI}{\rho a}}$$

where

V = vehicle velocity

l = span length

ρ = mass density [slugs in.⁻³]

a = guideway cross-sectional area

For our guideway,

$$T_{\text{transit}} = \frac{\pi}{2Vl} \sqrt{\sum \frac{EI}{\rho a}} = 4.76$$

For $T = 4.76$, the maximum dynamic deflection of the guideway is about 1.2 times the maximum static, i.e.

$$\Delta_{\text{dyn max}_1} = 1.2 \Delta_{\text{stat}} = 0.0029 \text{ in.}$$

Bolt Spacing on Lexan:

The following analysis was used to determine the appropriate bolt-spacing such that no buckling of the rails would occur during thermal transients at the track. According to Euler,

$$p_{\text{cr}} = \frac{\pi^2 EI}{L_{\text{cr}}^2}$$

Therefore the critical bolt spacings for a given temperature change are:

$\Delta\theta$ [°F]	10	20	30	40	50	60	70	80
L_{cr} [in]	59	41	34	29	26	24	22	21

A bolt-spacing of 20 inches has been chosen for safety.

Bolt-Spacing for Aluminum Channel:

Similarly, for aluminum bolted to steel,

$\Delta\theta$ [°F]	10	20	30	40	50	60	70	80
L_{cr} [in]	91	64	52	45	41	37	34	32

A bolt-spacing of 2 feet has been chosen.

Alignment:

Vertical alignment is achieved by adjusting the vertical floor studs.

Lateral alignment and gauge are set by moving the aluminum sections along the CRS plate. We are currently developing our alignment systems, which will consist of:

- a) Selection of adjustment points and tolerances using statistical models developed in [10].
- b) Selection of primary alignment instrumentation, possibly a laser transit with ± 0.0025 accuracy over 300 feet.
- c) Design of secondary instrumentation, such as a profilometer, to periodically check the track irregularity without tedious point-by-point measurements.

TABLE 2
TRACK STRUCTURE STATIC DEFLECTIONS

Assumed Deflection Shape

Maximum Design Deflection, 10^{-3} inches

Section	Assumed Deflection Shape	Maximum Design Deflection, 10^{-3} inches
1) Aluminum Extrusion		1.2
2) Aluminum Extrusion		7.2
3) Aluminum Extrusion	1) + 2)	8.4
4) Steel Channel**		1.0
5) Steel Channel		1.4
6) Steel Channel	4) + 5)	2.4
7) Assembled Box Section		4.0

(Box in torsion, side force applied midspan between piers)

* Conservative estimate since section is backed by cold-rolled steel plate.

** Where precamber exists in channels, camber will be oriented up to offset sag in beam.

DESIGN OF THE EXPERIMENT:

CO-ORDINATE SYSTEMS

Summary:

The use of wheelset, rail, and contact patch oriented coordinate systems is discussed, in terms of the impacts on experimental design and data reduction procedures.

Axis Systems:

Three axis systems are used in this experiment: the wheelset axes, the rail axes and the contact axes. They are based on the axis systems given in A Reexamination of the Derailment Properties of a Railway Wheelset, by Gilchrist and Brickle [6].

All forces and moments are applied to the wheelset and are positive in the positive axis directions. Moments are given from the forces by using the right hand rule.

Wheelset Axes superscript: -

axes: x^- , y^- , z^-

forces: F_x^- , F_y^- , F_z^-

moments: M_x^- , M_y^- , M_z^-

Rail Axes superscript: +

axes: x^+ , y^+ , z^+

forces: F_x^+ , F_y^+ , F_z^+

moments: M_x^+ , M_y^+ , M_z^+

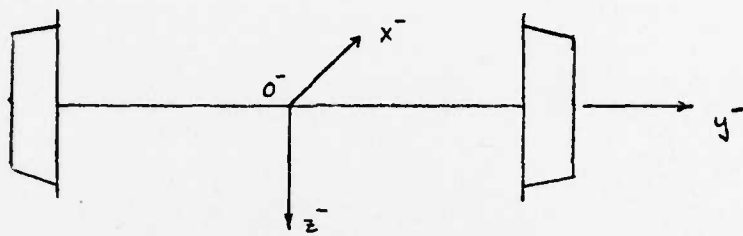
When no superscript is used the expression refers to either of the above axis systems.

Contact Axes subscripts: 1, 2, 3

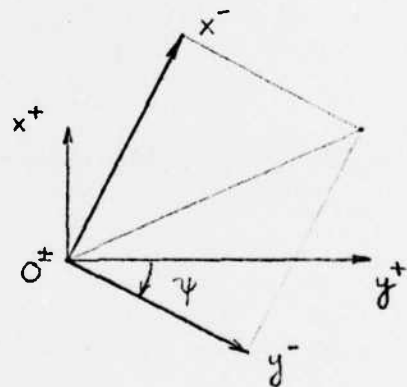
axes: c_1, c_2, c_3

forces: F_1, F_2, F_3

The subscripts l and r refer to the left and right wheels when viewed in the $0^- x^-$ direction.



The origins and z axes of the wheelset and rail axes coincide ($0^+ z^+ = 0^- z^-$), and the wheelset axes are given from the rail axes by a rotation ψ as shown below:



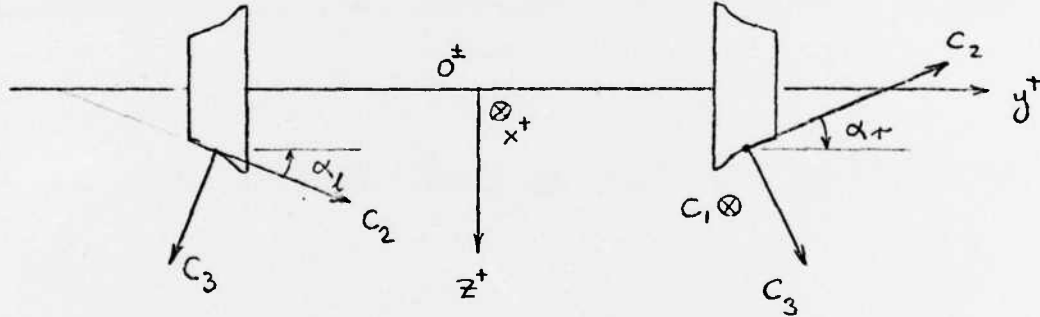
Rail to Wheelset

$$\begin{bmatrix} \cos \psi & \sin \psi & 0 \\ -\sin \psi & \cos \psi & 0 \\ 0 & 0 & 1 \end{bmatrix} \begin{bmatrix} x^+ \\ y^+ \\ z^+ \end{bmatrix} = \begin{bmatrix} x^- \\ y^- \\ z^- \end{bmatrix}$$

Wheelset to Rail

$$\begin{bmatrix} \cos \psi & -\sin \psi & 0 \\ \sin \psi & \cos \psi & 0 \\ 0 & 0 & 1 \end{bmatrix} \begin{bmatrix} x^- \\ y^- \\ z^- \end{bmatrix} = \begin{bmatrix} x^+ \\ y^+ \\ z^+ \end{bmatrix}$$

The transformation from rail to contact axes is also a rotation. There are two sets of contact axes: one for the left wheel and one for the right. c_1 is parallel to the track and tangent to the contact patch. c_2 is tangent to the patch and perpendicular to c_1 . c_3 is normal to the contact patch. The relationship between the contact and rail axes is shown in the diagram:



The transformations are as follows:

Rail to contact

$$\begin{bmatrix} 1 & 0 & 0 \\ 0 & \cos \alpha & -\sin \alpha \\ 0 & \sin \alpha & \cos \alpha \end{bmatrix} \begin{bmatrix} x^+ \\ y^+ \\ z^+ \end{bmatrix} = \begin{bmatrix} c_1 \\ c_2 \\ c_3 \end{bmatrix}$$

Contact to Rail

$$\begin{bmatrix} 1 & 0 & 0 \\ 0 & \cos \alpha & \sin \alpha \\ 0 & -\sin \alpha & \cos \alpha \end{bmatrix} \begin{bmatrix} c_1 \\ c_2 \\ c_3 \end{bmatrix} = \begin{bmatrix} x^+ \\ y^+ \\ z^+ \end{bmatrix}$$

These transformations can be used for both wheel's if we define $\alpha_r > 0$ and $\alpha_l < 0$. To get from rail or wheelset axes to constant axes there is also a translation involved which is not fixed but moves with the constant points.

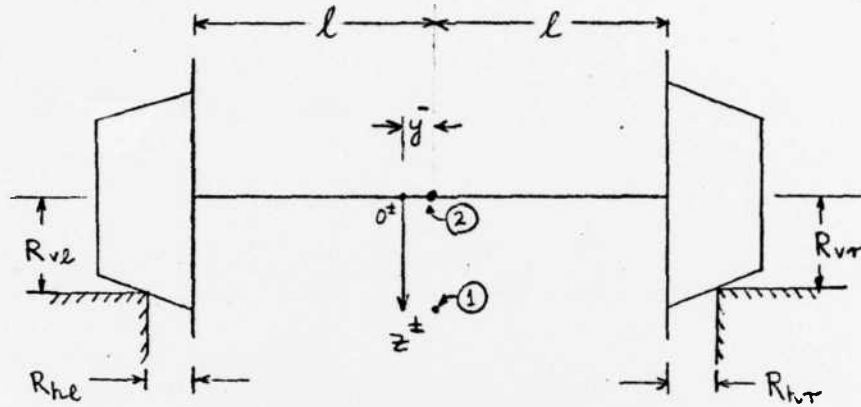
Experimental Design:

The purpose of the following analysis is to determine which of the three axis systems is most suitable for data analysis and which is best for force application. The previous transformations are used to change from one system to the others. The criterion for selection is simplicity of the resulting equations and ease of implementation.

The experiment consists of a railway with a carriage serving as an inertial reference and measuring device. A single wheelset is mounted on the carriage through a set of instrumented linkages. In the first experiment the relationship between M_z , ψ , F_y and y is compared with theory. If these parameters are known, and all others are held constant, the forces at the contact points can be found and measured results compared with Kalker's theory. F_y and ψ were chosen as the independent parameters. Once they are set M_z and y can be measured.

There are two choices for the force application point. It can be applied at the geometric center of the wheelset or a distance R_o below it.

The forces can be applied in wheelset axes or in rail axes. The choices for the force application point are shown below.



Points (1) and (2) correspond to the force application points:

$$(1) \vec{A}^- = (0, y^-, R_o^-)$$

$$(2) \vec{A}^- = (0, y^-, 0)$$

$$\vec{c}_r^- = (0, L_r + y^-, R_{vr}) \quad \text{where } L_r = l + R_{hr}$$

$$\vec{c}_\ell^- = (0, L_\ell + y^-, R_{v\ell}) \quad \text{where } L_\ell = - (l + R_{hl})$$

It is assumed that the roll angle is very small and that $R_o^- \approx R_{v\ell}^- \approx R_{vr}^-$.

The above equations yield:

$$\text{Point (1)} \quad \vec{R}_r^- = \vec{c}_r^- - \vec{A}^- = (0, L_r, 0)$$

$$\vec{R}_\ell^- = \vec{c}_\ell^- - \vec{A}^- = (0, L_\ell, 0)$$

$$\text{Point (2)} \quad \vec{R}_r^- = (0, L_r, R_{vr})$$

$$\vec{R}_\ell^- = (0, L_\ell, R_{v\ell})$$

The moment at these points is calculated by:

$$\vec{M}_y + \vec{R}_l \times \vec{F}_l + \vec{R}_r \times \vec{F}_r = 0$$

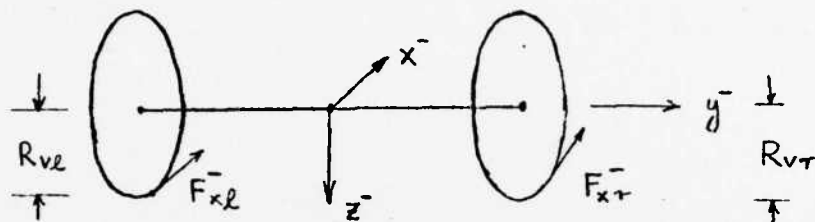
Using the first point eliminates the M_y component whereas using the second gives a moment with three components. Therefore, Point (1) will be used.

From a data analysis standpoint, there is no reason to choose between the wheelset and rail axis systems. Therefore, the choice of axis system for the force application requires consideration of the implementation. If the forces are applied in the rail system, they have fixed directions with respect to the carriage and are easier to adjust. If the forces are applied in the wheelset system, then the directions of the forces must follow the directions of the wheelset. This choice has no effect in the static case but will influence the dynamic case. In addition it is more likely that the rail system models the real case properly since the bulk motion of the car body is in the forward and lateral directions with respect to the rail system.

Once the axis systems are defined we can write three force equations giving F_x , F_y , F_z and two moment equations for M_x and M_z in terms of F_{r1} , F_{r2} , F_{r3} , $F_{\ell1}$, $F_{\ell2}$, $F_{\ell3}$. The equation of M_y is not given readily since the bearings allow the wheels to rotate and no moment is transmitted. In order to find the sixth equation, we can follow two approaches. One is to assume that both wheels have the same forces acting on them. This is only true for coned wheels. The other approach is to measure the moment between the two wheels. This is done by mounting strain gages along the

axle of the wheelset. Referring to the drawing below, the equation is:

$$M_y = F_{xr} R_{vr} - F_{xl} R_{vl}$$



This gives us the additional information necessary to complete the wheelset-equations. After applying the appropriate transformations and making a small angle approximation for ψ , the equations are written as shown in Figure 11.

Computational Method:

A computational method has been proposed for use in experimental design and subsequent data analysis, shown schematically in Figure 12. The method consists of the following elements:

- a) Using wheel and rail profile data the kinematic relationships between y and contact point, roll angle, rolling radii, and profile curvatures are determined [12].
- b) Using Hertz contact theory, and estimating normal forces F_3 in the left and right contact planes, the dimensions of the contact ellipse a, b are determined.
- c) Estimating axle speed Ω , the relative velocities v_1, v_2 , and ω_3 are calculated. From Kalker's theory the lateral and tangential creep forces are computed.

- d) Equilibrium in vertical plane passing through the wheelset axle determines forces F_3 (left and right).
- e) The forces \vec{F}_l and \vec{F}_r in the contact planes are transformed using the (6×6) matrix to give forces and moments in the wheelset coordinate system.
- f) The estimated axle speed Ω is iterated until M_y^- is zero (by definition). The normal forces F_3 are also iterated until their values converge.

Experimental Parameters:

Preset conditions for each run are:

- a) V^+ Forward velocity
- b) ψ Yaw angle
- c) F_y^+ Lateral force
- d) F_z^+ Vertical force
- e) M_x^+ Roll moment

Measured variables are:

- f) y^- Lateral displacement
- g) M_y^* Axle twisting moment
- h) Ω Axle speed
- i) M_z^+ Yaw moment
- j) F_x^+ Towing force

In the computational process, variables a, b, d, and f are inputs; the remainder are calculated.

$$\begin{bmatrix}
-1 & -\psi \cos \alpha_\lambda & -\psi \sin \alpha_\lambda & -1 & -\psi \cos \alpha_r & -\psi \sin \alpha_r \\
\psi & -\cos \alpha_\lambda & -\sin \alpha_\lambda & \psi & -\cos \alpha_r & -\sin \alpha_r \\
0 & \sin \alpha_\lambda & -\cos \alpha_\lambda & 0 & \sin \alpha_r & -\cos \alpha_r \\
0 & L_\lambda \sin \alpha_\lambda & -L_\lambda \cos \alpha_\lambda & 0 & L_r \sin \alpha_r & -L_r \cos \alpha_r \\
-R_{v\lambda} & -R_{v\lambda} \psi \cos \alpha_L & -R_{v\lambda} \psi \sin \alpha_L & R_{vr} & R_{vr} \psi \cos \alpha_r & R_{vr} \psi \sin \alpha_r \\
L_\lambda & L_\lambda \psi \cos \alpha_\lambda & L_\lambda \psi \sin \alpha_L & L_r & L_r \psi \cos \alpha_r & L_r \psi \sin \alpha_r
\end{bmatrix}
=
\begin{bmatrix}
F_x \\
F_y \\
F_z \\
M_x \\
M_y \\
M_z
\end{bmatrix}$$

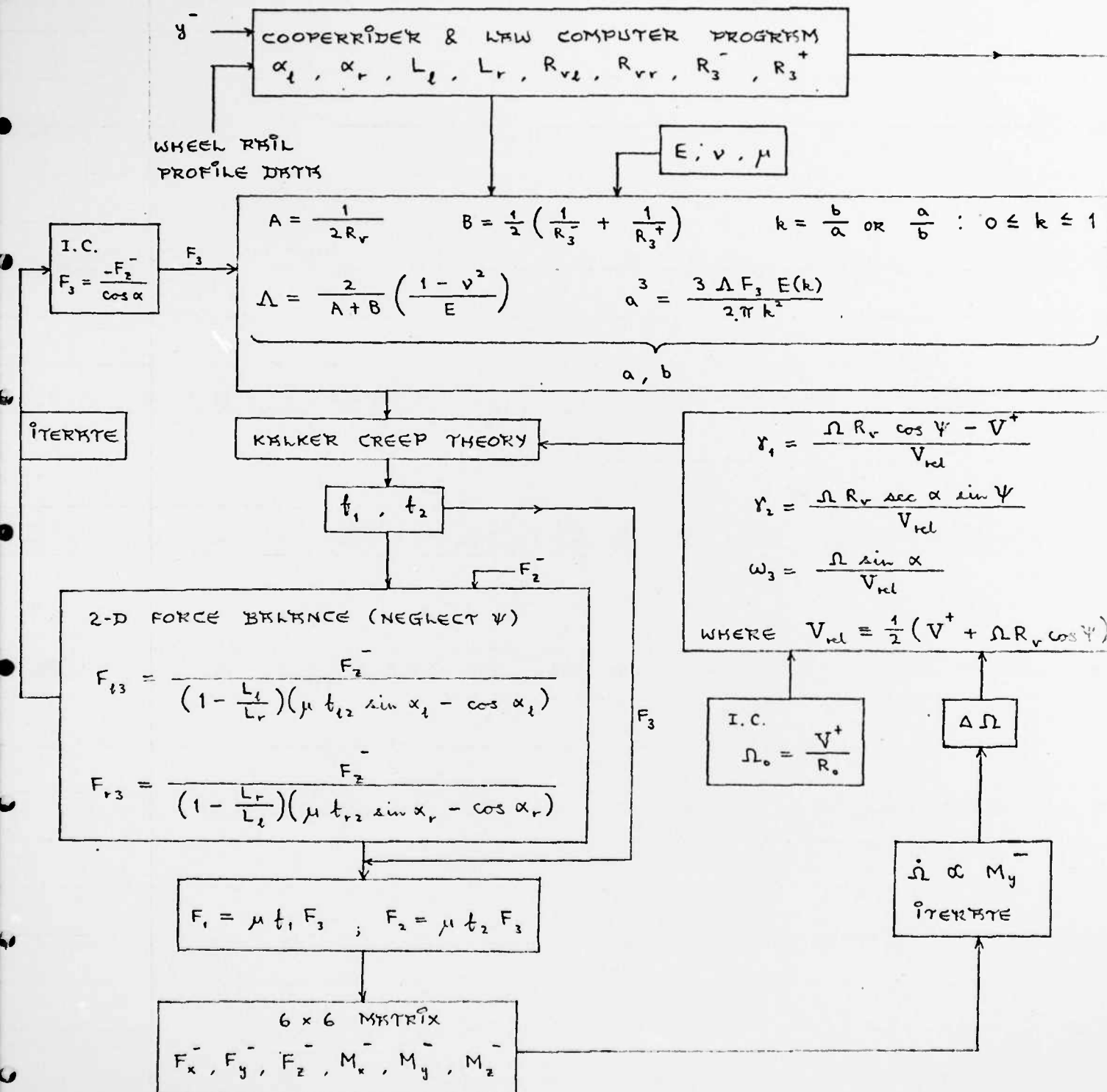
Figure 11 - Matrix conversion of contact plane forces to wheelset-coordinate forces and moments.

PETER WAY
WILSON TSU

FIGURE 12

EXPERIMENTAL ALGORITHM

EX/12/MCMLXXVI KNOWN QUANTITIES : F_z , y , ψ , v .



R_3^+ = lateral rail-head radius at contact point.

R_3 = lateral wheel radius at contact point.

REFERENCES

1. Verneulen, P.J. and Johnson, K.L., "Contact of Nonspherical Elastic Bodies Transmitting Tangential Forces." ASME Trans., J. of Applied Mechanics, 1964, pp. 338-340.
2. Karamchandani, K.C., et. al., "Friction-Creep and Wear Studies for Steel Wheel and Rail." Illinois Institute of Technology Report No. IIT-TRANS-75-1, May 1975.
3. Sciammarella, C., et. al., "Study of Friction and Creep between Steel Wheels and Rail," Illinois Institute of Technology Report No. IIT-TRANS-76-2, March 1976.
4. Ollerton, E., "Stresses in the Contact Zone." Proc. Inst. Mech. Engrs., Vol. 178, pt. 3E., pp. 161-171.
5. Hobbs, A.E.W., "A Survey of Creep." British Railways Research Dept. No. DYN 52, April 1967.
6. Gilchrist, A.O. and Brickle, B.V., "A Re-examination of the Derailment Properties of a Railway Wheelset." In The Dynamics of Vehicles on Roads and Railway Tracks, ed. H. Pacejka, Swets and Zeitlinger, B.V., Amsterdam, 1976.
7. Matsudarra, T. et. al., "Problems on Hunting of Railway Vehicles on Test Stand." ASME Paper No. 68-WA/RR-2.
8. Barwell, F.T. and Woolacott, R.G., "The N.E.L. Contribution to Adhesion Studies." Proc. Conf. Adhesion. J. Mech. E., London, 1963, pp. 145-160.
9. Wickens, A.H., "The Dynamics of Railway Vehicles on Straight Track: Fundamental Considerations of Lateral Stability." Proc. J. Mech. Engr. 1965, Vol. 180, Pt. 3F., pp. 29-44.
10. Hullender, D.A., et.al. "Analytical Models for Guideway Surface Irregularities and Terrain Smoothing."
11. Chiu, W., and Wormley, D.N., "Influence of Vehicle and Distributed Guideway Parameters on High-Speed Vehicle-Guideway Dynamic Interaction." Trans. ASME, J. Basic Engr., March 1971, pp. 25-34.
12. Cooperrider, N.K., Law, E.H., et.al., "Analytical and Experimental Determination of Nonlinear Wheel/Rail Geometric Constraints," presented at 1975 ASME Winter Annual Meeting.

WORK PLAN

1976 1977
7 8 9 10 11 12 1 2 3 4 5 6

I. Apparatus Design and Fabrication

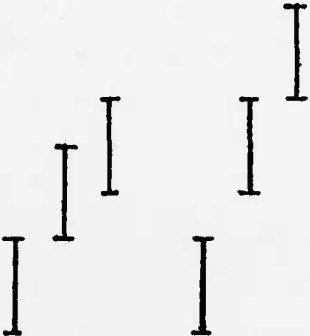
A. Track Structure:

1. Design
2. Material Acquisition
3. Installation

B. Rails:

1. Design
2. Fabrication
3. Installation

C. Carriage and Wheelset:



1. Design
2. Fabrication
3. Installation

D. Roller Rig:

1. Design and Fabrication
2. Alignment
3. Maintenance

E. Track Alignment

1. Laser design
2. Alignment in place
3. Maintenance



II. Experimentation

A. Roller Rig:

1. Tangential creep

2. Lateral creep

3. Spin creep (if time permits)



B. Tangent Track:

1. Constant ψ tests

2. Variable ψ tests (if time permits)



III. Analysis:

A. Comparison of Roller Rig Tests with Theory

B. "On Paper" Experimental Design

C. Comparison of Tangent Track Experiment Data with Theory

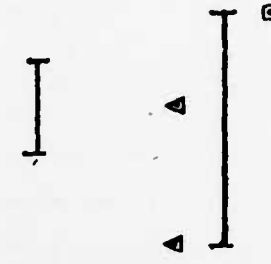


IV. Reporting:

A. Quarterly Reports

B. Site Visits from DOT and other Outside Professionals

C. Final Report



Personnel Assignments

Faculty: Larry J. Sweet (Principal investigator, all design, IIB, III, IV)
Howard C. Curtiss, Jr. (IIC, IIB)

Graduate Student: Joseph Sivak (Fabrications, IIB, IIIB, IIIC)
Undergraduate Students: Alan Au '77 Thomas Swift '76
Ann Bunnett '78 Peter Way '77

Prentiss Hall '79 Robert McKillip '78

Technical Staff: William Putman (All design, IIB)
T. Griffith (Design and fabrication, IIB)

PERSONNEL ASSIGNMENTS

(All design, IIA, IIB, IIIA, IIIB)

END

FILMED

9-83

DTIC